Geophys. J. Int. (2000) **142,** 000–000

An Arbitrary High Order Discontinuous Galerkin Method for Elastic Waves on Unstructured Meshes III: Viscoelastic Attenuation

Martin Käser[1], Michael Dumbser[1,3], Josep de la Puente[2], Heiner Igel[2]

[1] *Department of Civil and Environmental Engineering, University of Trento, Trento, Italy*
[2] *Department of Earth and Environmental Sciences, Section Geophysics, Ludwig-Maximilians-Universität, München, Germany*
[3] *Institut für Aerodynamik und Gasdynamik, Universität Stuttgart, Germany*

Accepted 1999 November 11. Received 1999 October 6; in original form 1999 August 3

SUMMARY

We present a new numerical method to solve the heterogeneous anelastic, seismic wave equations with arbitrary high order accuracy in space and time on three dimensional unstructured tetrahedral meshes. Using the velocity-stress formulation provides a linear hyperbolic system of equations with source terms that is completed by additional equations for the anelastic functions including the stain history of the material. These additional equations result from the rheological model of the generalized Maxwell body and permit the incorporation of realistic attenuation properties of viscoelastic material accounting for the behaviour of elastic solids and viscous fluids. The proposed method combines the Discontinuous Galerkin (DG) Finite Element method with the *ADER* approach using *A*rbitrary high order *DER*ivatives for flux calculation. The DG approach, in contrast to classical Finite Element methods, uses a piecewise polynomial approximation of the numerical solution which allow for discontinuities at element interfaces. Therefore, the well-established theory of numerical fluxes across element interfaces obtained by the solution of Riemann problems can be applied as in the finite volume framework. The main idea of the ADER time integration approach is a Taylor expansion in time in which all time derivatives are replaced by space derivatives using the so-called Cauchy-Kovalewski procedure which makes extensive use of the governing PDE. Due to the ADER time integration technique the same approximation order in space and time is achieved automatically and the method is a one-step scheme advancing the solution for one time step without intermediate stages. To this end, we introduce a new unrolled recursive algorithm for efficiently computing the Cauchy-Kovalewski procedure by making use of the sparsity of the system matrices. The numerical convergence analysis demonstrates that the new schemes provide very high order accuracy even on unstructured tetrahedral while computational cost and storage space for a desired accuracy can be reduced when applying higher degree approximation polynomials. In addition, we investigate the increase in computing time, when the number of attenuation mechanisms due to the generalized Maxwell body are increased. An application to a well-acknowledged test case and comparisons with analytic and reference solutions, obtained by different well-established numerical methods, confirm the performance of the proposed method. Therefore, the development of the highly accurate ADER-DG approach for tetrahedral meshes including viscoelastic material provides a numerical technique to approach three-dimensional wave propagation problems including realistic attenuation and complex geometry.

Key words: viscoelasticity, attenuation, Discontinuous Galerkin, high order accuracy, unstructured meshes

1 INTRODUCTION

Modern numerical methods for the simulation of seismic wave propagation are becoming more accurate, can handle complex three-dimensional geometries and provide increasingly important tools to simulate more realistic ground motion scenarios for seismic risk assessment. Therefore, second-order effects such as attenuation and dispersion, which strongly affect the seismic wave field, have to be incorporated to correctly model the wave amplitudes and phases of a fully three-dimensional seismic wave field. A successful approach of modeling realistic atten-

uation is the approximation of the material as a viscoelastic medium that combines the behaviour of both, elastic solids and viscous fluids. Hereby, it is important that the earth's internal friction, i.e. the measure of attenuation, is nearly constant over a wide seismic frequency range. This is due to the composition of the earth's polycristalline material consisting of different minerals. The superposition of these microscopic physical attenuation processes leads to a flat attenuation band, see (Liu, Anderson & Kanamori 1976; Stein & Wysession 2003).
The stress-strain relation for a linear isotropic viscoelastic medium is given by the so-called Boltzmann principle (causality principle), that states that the stress at a given time t depends on the entire strain history until time t, which mathematically is represented by a time convolution of a relaxation function and the strain rate, as outlined in (Moczo, Kristek & Halada 2004). As the integration of this stress-strain relation in the time domain is intractable in a numerical computation, Day & Minster (1984) transformed the stress-strain relation in the time domain into a differential form using Padé approximations. They obtained n differential equations for n additional *internal variables*, which replace the convolution integral. These equations have to be solved in addition to the elastic wave equations. Furthermore, the sum of the internal variables multiplied with anelastic coefficients leads to additional viscoelastic terms for the elastic stresses. This way storage requirements and computing times were significantly increased.
Emmerich & Korn (1987) improved this approach by considering the rheology of a *generalized Maxwell body* and showed that their method is superior in accuracy and computational efficiency. They chose the relaxation frequencies logarithmically equidistant in the frequency band of interest and used a least-square method to fit arbitrary quality factor laws.
Independently, a different approach in (Carcione, Kosloff & Kosloff 1988; Carcione & Cavallini 1994) assumed a *generalized Zener body* and introduced additional first order differential equations for *memory variables*. After these revolutionary publications authors incorporating realistic viscoelastic attenuation in time domain methods used the concepts of the generalized Maxwell or generalized Zener body. Recent work by Moczo & Kristek (2005) reviewed both models and showed that indeed both approaches are equivalent.
After Emmerich (1992) applied the viscoelastic models for the P-SV case, Moczo *et al.* (1997) presented a hybrid two-step method for simulating P-SV seismic motion in inhomogeneous viscoelastic structures with free surface topography combining discrete-wavenumber (DW) (Bouchon 1981), finite element (FE) (Marfurt 1984) and finite-difference (FD) (Moczo & Bard 1993) methods. Later, different work, e.g. (Day 1998; Day & Bradley 2001; Kristek & Moczo 2003), addressed the basic theoretical and algorithmic aspects of a memory-efficient implementation of realistic attenuation based on a viscoelastic material with material discontinuities mainly for the staggered-grid finite difference approach.
In this paper, we incorporate realistic attenuation by viscoelastic material into the high-order Discontinuous Galerkin (DG) approach. Originally developed in (Reed & Hill 1973), Dumbser (2005) and Dumbser & Munz (2005a; 2005b) combined the DG method with the *ADER* approach of (Toro, Millington & Nejad 2001; Titarev & Toro 2002; Toro & Titarev 2002) for accurate time integration using *A*rbitrary high order *DER*ivatives. This new highly accurate numerical method was then introduced for the simulation of seismic wave propagation on unstructured meshes for two and three space dimensions (Käser & Dumbser 2006; Dumbser & Käser 2006). In this new approach we approximate the unknown solution as well as the additional anelastic functions, provided by the generalized Maxwell body, inside each tetrahedral element by a polynomial, whose coefficients - the degrees of freedom - are advanced in time. Hereby, the solution can be *discontinuous* across the element interfaces, which allows to incorporate the well-established ideas of numerical flux functions from the finite volume framework as shown in (Käser & Dumbser 2006).

The paper is structured as follows. In Section 2 we introduce the system of the three-dimensional anelastic wave equations in velocity-stress formulation including attenuation due to viscoelasticity. The resulting DG method is briefly explained in Section 3 together with the ADER time integration approach. However, to avoid repetition we strongly refer to previous work on the purely elastic case in (Dumbser & Käser 2006). Furthermore, we give a new and more efficient formulation for the required Cauchy-Kovalewski procedure. Results of the numerical convergence rates of the proposed ADER-DG scheme for anelastic wave propagation on tetrahedral meshes are shown in Section 4. In Section 5 we demonstrate the improvement of the approximation of a frequency-independent $\mathcal{Q}$-law when increasing the number n of attenuation mechanisms of the generalized Maxwell body. Furthermore, we analyse the additional CPU time requirements for different orders of accuracy of the ADER-DG schemes. Finally, in Section 6, we present a comparison of our results with those published after an acknowledged three-dimensional benchmark test of the Pacific Earthquake Engineering Research Center (Day, Bielak, Dreger, Graves, Larsen, Olsen & Pitarka 2003) providing an analytic and a number of reference solutions obtained by well-established codes of other research institutions. In particular, we compare the results for different orders of accuracy combined with different numbers of attenuation mechanisms.

2 ANELASTIC WAVE EQUATIONS

The anelastic wave propagation can be described by modifying the constitutive relation, i.e. Hooke's Law, as shown in (Moczo, Kristek & Halada 2004) and transforming it into the frequency domain. The relation between stresses $\vec{\sigma} = (\sigma_{xx}, \sigma_{yy}, \sigma_{zz}, \sigma_{xy}, \sigma_{yz}, \sigma_{xz})^T$ and strains $\vec{\varepsilon} = (\varepsilon_{xx}, \varepsilon_{yy}, \varepsilon_{zz}, \varepsilon_{xy}, \varepsilon_{yz}, \varepsilon_{xz})^T$ in the case of linear viscoelasticity can then be written as

$$\vec{\sigma_i}(\omega) = M_{ij}(\omega)\vec{\varepsilon_j}(\omega) \tag{1}$$

where M_{ij} is a matrix including complex, frequency-dependent viscoelastic moduli. In general M_{ij} has 21 independent entries, however, for the isotropic case they reduce to the two Lamé parameters $\lambda = \lambda(\omega)$ and $\mu = \mu(\omega)$.

The rheological model that defines the parameters of M_{ij} has to have a physically feasible expression that, in addition, reproduces the expected results of stress and strain damping as well as experimental observation of strain response to stress loads. In (Liu, Anderson & Kanamori 1976) a superposition of different relaxation mechanisms is proposed as a way to fulfill both conditions. As introduced in (Emmerich & Korn 1987) and clearly outlined in (Moczo & Kristek 2005) we can express the viscoelastic moduli as a combination of n mechanisms (so-called Maxwell Bodies) as

$$\lambda(\omega) = \lambda^U \Big(1 - \sum_{\ell=1}^{n} \frac{Y_\ell^\lambda \omega_\ell}{\omega_\ell + i\omega}\Big)\,, \tag{2}$$

$$\mu(\omega) = \mu^U \Big(1 - \sum_{\ell=1}^{n} \frac{Y_\ell^\mu \omega_\ell}{\omega_\ell + i\omega}\Big)\,, \tag{3}$$

where $\lambda^U = \lim_{\omega\to\infty} \lambda(\omega)$ and $\mu^U = \lim_{\omega\to\infty} \mu(\omega)$ are the unrelaxed Lamé parameters as used in purely elastic media. The Y_ℓ^λ and Y_ℓ^μ are the anelastic coefficients to be determined and ω_ℓ are the relaxation frequencies of the different mechanisms.
In general, given a viscoelastic modulus, e.g. the shear modulus $\mu(\omega)$, the quality factor $\mathcal{Q}(\omega)$ is defined as

$$\mathcal{Q}(\omega) = \frac{Re(\mu(\omega))}{Im(\mu(\omega))}\,. \tag{4}$$

Inserting the shear modulus $\mu(\omega)$ from (3) into (4) leads to

$$\mathcal{Q}_\mu^{-1}(\omega) = \sum_{\ell=1}^{n} \frac{\omega_\ell\omega + \omega_\ell^2 \mathcal{Q}_\mu^{-1}(\omega)}{\omega_\ell^2 + \omega^2} Y_\ell^\mu\,. \tag{5}$$

The equation (5) can be used to fit any $\mathcal{Q}(\omega)$-law as shown in (Emmerich & Korn 1987; Moczo, Kristek & Halada 2004). Observations show, that the quality factor $\mathcal{Q}$ is approximately constant over a large frequency range of interest for most geophysical applications. They propose, that good approximations can be obtained by choosing n relaxation frequencies ω_ℓ, $\ell = 1, ..., n$, that cover the frequency range of interest logarithmically equidistantly. They suggest to use $2n-1$ known values $\mathcal{Q}(\tilde{\omega}_k)$ at frequencies $\tilde{\omega}_k$, $k = 1, ..., 2n-1$, with $\tilde{\omega}_1 = \omega_1$ and $\tilde{\omega}_{2n-1} = \omega_n$ and solve the overdetermined system in (5) for the anelastic coefficients Y_ℓ^μ by the least square method. A more detailed discussion of the choice of frequency ranges and the corresponding sampling frequencies can be found in (Graves & Day 2003).
In practice and analogous to the seismic P- and S-wave velocities, we have quality factors $\mathcal{Q}_P$ and $\mathcal{Q}_S$ that describe the different degree of attenuation for the different wave types. Therefore, from (5) we can also derive anelastic coefficients Y_ℓ^P and Y_ℓ^S for viscoelastic P- and S-wave propagation by solving the systems

$$\mathcal{Q}_\nu^{-1}(\omega_k) = \sum_{\ell=1}^{n} \frac{\omega_\ell\omega_k + \omega_\ell^2 \mathcal{Q}_\nu^{-1}(\omega_k)}{\omega_\ell^2 + \omega_k^2} Y_\ell^\nu\,, \qquad \text{with} \quad \nu = P, S\,, \quad \text{and} \quad k = 1, ..., 2n-1\,. \tag{6}$$

In the following, however, it is more convenient to express the anelastic coefficients in terms of the Lamé parameters λ and μ, which are obtained by the transformation

$$Y_\ell^\lambda = \Big(1 + \frac{2\mu}{\lambda}\Big) Y_\ell^P - \frac{2\mu}{\lambda} Y_\ell^S\,, \qquad\qquad Y_\ell^\mu = Y_\ell^S\,, \tag{7}$$

following directly from (2) and (3) as the relation of physical parameters, e.g. elastic parameters or velocities, corresponds to the purely elastic case due to the linearity of the expressions in (2) and (3).
As shown in (Kristek & Moczo 2003; Moczo & Kristek 2005) we define a new set of variables, which are independent on the material properties, called the *anelastic functions* $\vec{\vartheta}^\ell = (\bar{\vartheta}_{xx}^\ell, \bar{\vartheta}_{yy}^\ell, \bar{\vartheta}_{zz}^\ell, \bar{\vartheta}_{xy}^\ell, \bar{\vartheta}_{yz}^\ell, \bar{\vartheta}_{xz}^\ell)^T$, which contain the time history of the strain in the form

$$\bar{\vartheta}_j^\ell(t) = \omega_\ell \int_{-\infty}^{t} \varepsilon_j(\tau) e^{-\omega_\ell(t-\tau)}\, d\tau\,. \tag{8}$$

Using (8)and applying the inverse Fourier transform to the viscoelastic modulus M_{ij} as outlined in detail in (Moczo & Kristek 2005) the stress-strain relation (1) can be written in the time domain in the form

$$\sigma_{ij} = \lambda\varepsilon_{kk}\delta_{ij} + 2\mu\varepsilon_{ij} - \sum_{\ell=1}^{n} (\lambda Y_\ell^\lambda \bar{\vartheta}_{kk}^\ell \delta_{ij} + 2\mu Y_\ell^\mu \bar{\vartheta}_{ij}^\ell)\,, \qquad \text{with} \quad i, j, k \in [x, y, z] \tag{9}$$

where δ_{ij} is the Kronecker Delta and the equal-index summation convention applies to the index kk. The viscoelastic constitutive relation in (9) represents the elastic part minus the anelastic part depending on the anelastic coefficients Y_ℓ^λ and Y_ℓ^μ and the anelastic functions $\bar{\vartheta}_{ij}^\ell$. The remaining problem is the evolution of the anelastic functions $\bar{\vartheta}_{ij}^\ell$ in (8) in time. In fact, equation (8) is the solution of the partial differential equation

$$\frac{\partial}{\partial t}\bar{\vartheta}_j^\ell(t) + \omega_\ell \bar{\vartheta}_j^\ell(t) = \omega_\ell \varepsilon_j\,, \tag{10}$$

which completes the linear, hyperbolic system of the anelastic wave equations.
However, to express the equation system in the velocity-stress formulation it is convenient to redefine the anelastic functions in the form

$$\vartheta_j^\ell = \frac{\partial}{\partial t}\bar{\vartheta}_j^\ell\,. \tag{11}$$

Finally, using the equations of motion, the definition of strain ε_j and equations (9), (10) and (11) we can formulate the system of the anelastic wave equations as

$$
\begin{aligned}
\tfrac{\partial}{\partial t}\sigma_{xx} - (\lambda+2\mu)\tfrac{\partial}{\partial x}u - \lambda\tfrac{\partial}{\partial y}v - \lambda\tfrac{\partial}{\partial z}w &= \sum_{\ell=1}^{n} -(\lambda Y_\ell^\lambda + 2\mu Y_\ell^\mu)\vartheta_{xx}^\ell - \lambda Y_\ell^\lambda \vartheta_{yy}^\ell - \lambda Y_\ell^\lambda \vartheta_{zz}^\ell\,,\\
\tfrac{\partial}{\partial t}\sigma_{yy} - \lambda\tfrac{\partial}{\partial x}u - (\lambda+2\mu)\tfrac{\partial}{\partial y}v - \lambda\tfrac{\partial}{\partial z}w &= \sum_{\ell=1}^{n} -\lambda Y_\ell^\lambda \vartheta_{xx}^\ell - (\lambda Y_\ell^\lambda + 2\mu Y_\ell^\mu)\vartheta_{yy}^\ell - \lambda Y_\ell^\lambda \vartheta_{zz}^\ell\,,\\
\tfrac{\partial}{\partial t}\sigma_{zz} - \lambda\tfrac{\partial}{\partial x}u - \lambda\tfrac{\partial}{\partial y}v - (\lambda+2\mu)\tfrac{\partial}{\partial z}w &= \sum_{\ell=1}^{n} -\lambda Y_\ell^\lambda \vartheta_{xx}^\ell - \lambda Y_\ell^\lambda \vartheta_{yy}^\ell - (\lambda Y_\ell^\lambda + 2\mu Y_\ell^\mu)\vartheta_{zz}^\ell\,,\\
\tfrac{\partial}{\partial t}\sigma_{xy} - \mu(\tfrac{\partial}{\partial x}v + \tfrac{\partial}{\partial y}u) &= \sum_{\ell=1}^{n} -2\mu Y_\ell^\mu \vartheta_{xy}^\ell\,,\\
\tfrac{\partial}{\partial t}\sigma_{yz} - \mu(\tfrac{\partial}{\partial z}v + \tfrac{\partial}{\partial y}w) &= \sum_{\ell=1}^{n} -2\mu Y_\ell^\mu \vartheta_{yz}^\ell\,,\\
\tfrac{\partial}{\partial t}\sigma_{xz} - \mu(\tfrac{\partial}{\partial z}u + \tfrac{\partial}{\partial x}w) &= \sum_{\ell=1}^{n} -2\mu Y_\ell^\mu \vartheta_{xz}^\ell\,,\\
\rho\tfrac{\partial}{\partial t}u - \tfrac{\partial}{\partial x}\sigma_{xx} - \tfrac{\partial}{\partial y}\sigma_{xy} - \tfrac{\partial}{\partial z}\sigma_{xz} &= 0\,,\\
\rho\tfrac{\partial}{\partial t}v - \tfrac{\partial}{\partial x}\sigma_{xy} - \tfrac{\partial}{\partial y}\sigma_{yy} - \tfrac{\partial}{\partial z}\sigma_{yz} &= 0\,,\\
\rho\tfrac{\partial}{\partial t}w - \tfrac{\partial}{\partial x}\sigma_{xz} - \tfrac{\partial}{\partial y}\sigma_{yz} - \tfrac{\partial}{\partial z}\sigma_{zz} &= 0\,,\\
\tfrac{\partial}{\partial t}\vartheta_{xx}^1 - \omega_1\tfrac{\partial}{\partial x}u &= -\omega_1\vartheta_{xx}^1\,,\\
\tfrac{\partial}{\partial t}\vartheta_{yy}^1 - \omega_1\tfrac{\partial}{\partial y}v &= -\omega_1\vartheta_{yy}^1\,,\\
\tfrac{\partial}{\partial t}\vartheta_{zz}^1 - \omega_1\tfrac{\partial}{\partial z}w &= -\omega_1\vartheta_{zz}^1\,,\\
\tfrac{\partial}{\partial t}\vartheta_{xy}^1 - \tfrac{1}{2}\omega_1(\tfrac{\partial}{\partial x}v + \tfrac{\partial}{\partial y}u) &= -\omega_1\vartheta_{xy}^1\,,\\
\tfrac{\partial}{\partial t}\vartheta_{yz}^1 - \tfrac{1}{2}\omega_1(\tfrac{\partial}{\partial z}v + \tfrac{\partial}{\partial y}w) &= -\omega_1\vartheta_{yz}^1\,,\\
\tfrac{\partial}{\partial t}\vartheta_{xz}^1 - \tfrac{1}{2}\omega_1(\tfrac{\partial}{\partial z}u + \tfrac{\partial}{\partial x}w) &= -\omega_1\vartheta_{xz}^1\,,\\
&\vdots \quad \vdots\\
\tfrac{\partial}{\partial t}\vartheta_{xx}^n - \omega_n\tfrac{\partial}{\partial x}u &= -\omega_n\vartheta_{xx}^n\,,\\
\tfrac{\partial}{\partial t}\vartheta_{yy}^n - \omega_n\tfrac{\partial}{\partial y}v &= -\omega_n\vartheta_{yy}^n\,,\\
\tfrac{\partial}{\partial t}\vartheta_{zz}^n - \omega_n\tfrac{\partial}{\partial z}w &= -\omega_n\vartheta_{zz}^n\,,\\
\tfrac{\partial}{\partial t}\vartheta_{xy}^n - \tfrac{1}{2}\omega_n(\tfrac{\partial}{\partial x}v + \tfrac{\partial}{\partial y}u) &= -\omega_n\vartheta_{xy}^n\,,\\
\tfrac{\partial}{\partial t}\vartheta_{yz}^n - \tfrac{1}{2}\omega_n(\tfrac{\partial}{\partial z}v + \tfrac{\partial}{\partial y}w) &= -\omega_n\vartheta_{yz}^n\,,\\
\tfrac{\partial}{\partial t}\vartheta_{xz}^n - \tfrac{1}{2}\omega_n(\tfrac{\partial}{\partial z}u + \tfrac{\partial}{\partial x}w) &= -\omega_n\vartheta_{xz}^n
\end{aligned}
\tag{12}
$$

where n is the number of mechanisms used to approximate a frequency-independent $\mathcal{Q}$-law and ρ is the density. Note, that each mechanism adds 6 further equations, i.e. one for each stress component. Therefore, the system of the purely elastic three-dimensional wave equations consisting of 9 equations increases by $6n$ equations in the anelastic case, when n mechisms are used.

In the following, we assume that the viscoelastic material is described with the same number n of mechanisms throughout the computational domain. Therefore, the notation will be identical to previous work (Dumbser & Käser 2006) treating the purely elastic case.
The above system (12) of $n_v = 9 + 6n$ variables and equations can be written in the more compact form

$$
\frac{\partial Q_p}{\partial t} + \check{A}_{pq}\frac{\partial Q_q}{\partial x} + \check{B}_{pq}\frac{\partial Q_q}{\partial y} + \check{C}_{pq}\frac{\partial Q_q}{\partial z} = \check{E}_{pq}Q_q. \tag{13}
$$

Note, that the dimensions of the variable vector Q, the Jacobian matrices $\check{A}$, $\check{B}$, $\check{C}$ and the source matrix $\check{E}$ now depend on the number n of attenuation mechanisms. To keep the notation as simple as possible and without loss of generality, in the following we assume that the order of the equations in (13) is such, that $p, q \in [1, ..., 9]$ denote the elastic part and $p, q \in [10, ..., n_v]$, denote the anelastic part of the system as presented in (12). As the Jacobian matrices $\check{A}$, $\check{B}$ and $\check{C}$ as well as the source matrix $\check{E}$ are sparse and show some particular symmetry pattern and as their dimensions may become impractical for notation, we will use the block-matrix syntax.

Therefore, we decompose the Jacobian matrices as follows:

$$\check{A} = \begin{bmatrix} A & 0 \\ A_a & 0 \end{bmatrix} \in \mathbb{R}^{n_v \times n_v}, \quad \check{B} = \begin{bmatrix} B & 0 \\ B_a & 0 \end{bmatrix} \in \mathbb{R}^{n_v \times n_v}, \quad \check{C} = \begin{bmatrix} C & 0 \\ C_a & 0 \end{bmatrix} \in \mathbb{R}^{n_v \times n_v}, \tag{14}$$

where $A, B, C \in \mathbb{R}^{9\times 9}$ are the Jacobians of the purely elastic part as given in (Dumbser & Käser 2006). The matrices A_a, B_a, C_a include the anelastic part and exhibit themselves a block structure of the form:

$$A_a = \begin{bmatrix} A_1 \\ \vdots \\ A_n \end{bmatrix} \in \mathbb{R}^{6n\times 9}, \quad B_a = \begin{bmatrix} B_1 \\ \vdots \\ B_n \end{bmatrix} \in \mathbb{R}^{6n\times 9}, \quad C_a = \begin{bmatrix} C_1 \\ \vdots \\ C_n \end{bmatrix} \in \mathbb{R}^{6n\times 9}, \tag{15}$$

where each sub-matrix $A_\ell, B_\ell, C_\ell \in \mathbb{R}^{6\times 9}$, with $\ell = 1, ..., n$, contains the relaxation frequency ω_ℓ of the ℓ-th mechanism in the form:

$$A_\ell = \omega_\ell \cdot \begin{pmatrix} 0 & 0 & 0 & 0 & 0 & 0 & -1 & 0 & 0 \\ 0 & 0 & 0 & 0 & 0 & 0 & 0 & 0 & 0 \\ 0 & 0 & 0 & 0 & 0 & 0 & 0 & 0 & 0 \\ 0 & 0 & 0 & 0 & 0 & 0 & 0 & -\frac{1}{2} & 0 \\ 0 & 0 & 0 & 0 & 0 & 0 & 0 & 0 & 0 \\ 0 & 0 & 0 & 0 & 0 & 0 & 0 & 0 & -\frac{1}{2} \end{pmatrix}, \tag{16}$$

$$B_\ell = \omega_\ell \cdot \begin{pmatrix} 0 & 0 & 0 & 0 & 0 & 0 & 0 & 0 & 0 \\ 0 & 0 & 0 & 0 & 0 & 0 & 0 & -1 & 0 \\ 0 & 0 & 0 & 0 & 0 & 0 & 0 & 0 & 0 \\ 0 & 0 & 0 & 0 & 0 & 0 & -\frac{1}{2} & 0 & 0 \\ 0 & 0 & 0 & 0 & 0 & 0 & 0 & 0 & -\frac{1}{2} \\ 0 & 0 & 0 & 0 & 0 & 0 & 0 & 0 & 0 \end{pmatrix}, \tag{17}$$

$$C_\ell = \omega_\ell \cdot \begin{pmatrix} 0 & 0 & 0 & 0 & 0 & 0 & 0 & 0 & 0 \\ 0 & 0 & 0 & 0 & 0 & 0 & 0 & 0 & 0 \\ 0 & 0 & 0 & 0 & 0 & 0 & 0 & 0 & -1 \\ 0 & 0 & 0 & 0 & 0 & 0 & 0 & 0 & 0 \\ 0 & 0 & 0 & 0 & 0 & 0 & 0 & -\frac{1}{2} & 0 \\ 0 & 0 & 0 & 0 & 0 & 0 & -\frac{1}{2} & 0 & 0 \end{pmatrix}. \tag{18}$$

The matrix $\check{E}$ in (13) representing a reaction source that couples the anelastic functions to the original elastic system can be decomposed as

$$\check{E} = \begin{bmatrix} 0 & E \\ 0 & E' \end{bmatrix} \in \mathbb{R}^{n_v \times n_v}, \tag{19}$$

with E of the block structure

$$E = [E_1, \ldots, E_n] \in \mathbb{R}^{9\times 6n}, \tag{20}$$

where each matrix $E_\ell \in \mathbb{R}^{9\times 6}$, with $\ell = 1, ..., n$, contains the anelastic coefficients Y_ℓ^λ and Y_ℓ^μ of the ℓ-th mechanism in the form:

$$E_\ell = \begin{pmatrix} -\lambda Y_\ell^\lambda - 2\mu Y_\ell^\mu & -\lambda Y_\ell^\lambda & -\lambda Y_\ell^\lambda & 0 & 0 & 0 \\ -\lambda Y_\ell^\lambda & -\lambda Y_\ell^\lambda - 2\mu Y_\ell^\mu & -\lambda Y_\ell^\lambda & 0 & 0 & 0 \\ -\lambda Y_\ell^\lambda & -\lambda Y_\ell^\lambda & -\lambda Y_\ell^\lambda - 2\mu Y_\ell^\mu & 0 & 0 & 0 \\ 0 & 0 & 0 & -2\mu Y_\ell^\mu & 0 & 0 \\ 0 & 0 & 0 & 0 & -2\mu Y_\ell^\mu & 0 \\ 0 & 0 & 0 & 0 & 0 & -2\mu Y_\ell^\mu \\ 0 & 0 & 0 & 0 & 0 & 0 \\ 0 & 0 & 0 & 0 & 0 & 0 \\ 0 & 0 & 0 & 0 & 0 & 0 \end{pmatrix}. \tag{21}$$

The matrix E' in (19) is a diagonal matrix and has the structure

$$E' = \begin{bmatrix} E'_1 & & 0 \\ & \ddots & \\ 0 & & E'_n \end{bmatrix} \in \mathbb{R}^{6n\times 6n}, \tag{22}$$

where each matrix $E'_\ell \in \mathbb{R}^{6\times 6}$, with $\ell = 1, ..., n$, is itself a diagonal matrix containing only the relaxation frequency ω_ℓ of the ℓ-th mechanism on its diagonal, i.e. $E'_\ell = -\omega_\ell \cdot I$ with $I \in \mathbb{R}^{6\times 6}$ denoting the identity matrix.

3 THE NUMERICAL SCHEME

The computational domain $\Omega \in \mathbb{R}^3$ is divided into conforming tetrahedral elements $\mathcal{T}^{(m)}$ being addressed by a unique index (m). Furthermore, we suppose the matrices $\check{A}_{pq}$, $\check{B}_{pq}$, $\check{C}_{pq}$ and $\check{E}_{pq}$ in (13) to be piecewise constant inside an element $\mathcal{T}^{(m)}$.
As outlined in detail in (Dumbser & Käser 2006) for the purely elastic case, the construction of the ADER-DG scheme including viscoelastic attenuation remains basically the same. However, now we consider a larger linear hyperbolic system of equations and add the source terms as given in (12) or (13). Therefore, following exactly along the lines in (Dumbser & Käser 2006) and without repeating the rather tedious derivation of the numerical scheme, we now get the fully discrete one-step ADER-DG scheme of the form

$$
\begin{aligned}
& \left[\left(\hat{Q}_{pl}^{(m)} \right)^{n+1} - \left(\hat{Q}_{pl}^{(m)} \right)^{n} \right] |J| \, M_{kl} \quad + \\
+ \quad & \tfrac{1}{2} \sum_{j=1}^{4} \check{T}_{pq}^{j} \left(\check{A}_{qr}^{(m)} + \left| \check{A}_{qr}^{(m)} \right| \right) (\check{T}_{rs}^{j})^{-1} \, |S_j| \, F_{kl}^{-,j} \cdot I_{qlmn}(\Delta t) \left(\hat{Q}_{mn}^{(m)} \right)^{n} + \\
+ \quad & \tfrac{1}{2} \sum_{j=1}^{4} \check{T}_{pq}^{j} \left(\check{A}_{qr}^{(m)} - \left| \check{A}_{qr}^{(m)} \right| \right) (\check{T}_{rs}^{j})^{-1} \, |S_j| \, F_{kl}^{+,j,i,h} \cdot I_{qlmn}(\Delta t) \left(\hat{Q}_{mn}^{(m_j)} \right)^{n} - \\
- \quad & \check{A}_{pq}^{*} \, |J| \, K_{kl}^{\xi} \cdot I_{qlmn}(\Delta t) \left(\hat{Q}_{mn}^{(m)} \right)^{n} - \check{B}_{pq}^{*} \, |J| \, K_{kl}^{\eta} \cdot I_{qlmn}(\Delta t) \left(\hat{Q}_{mn}^{(m)} \right)^{n} - \check{C}_{pq}^{*} \, |J| \, K_{kl}^{\zeta} \cdot I_{qlmn}(\Delta t) \left(\hat{Q}_{mn}^{(m)} \right)^{n} = \\
= \quad & |J| \, \check{E}_{pq} \cdot I_{qlmn}(\Delta t) \left(\hat{Q}_{mn}^{(m)} \right)^{n} M_{kl}
\end{aligned}
\tag{23}
$$

to evolve the degrees of freedom $\hat{Q}_{pl}^{(m)}$ in element $\mathcal{T}^{(m)}$ from time level t^n to t^{n+1}. We remark that the total number of unknowns in the viscoelastic case now depends on the number of attenuation mechanisms, such that the index $p, q, r, s = 1, ..., n_v$.
However, in the following let us skip the element index (m) and have a closer look at the matrix $\left|\check{A}_{pq}\right|$ and the rotation matrix $\check{T}_{pq}^{j}$ used for the flux computation in (23).
Similar to (14) we find that

$$
\left|\check{A}\right| = \begin{bmatrix} |A| & 0 \\ A^{||} & 0 \end{bmatrix} \in \mathbb{R}^{n_v \times n_v},
\tag{24}
$$

where $|A| \in \mathbb{R}^{9\times 9}$ is identical to the one of the purely elastic part as given in (Dumbser & Käser 2006) and has the form

$$
|A| = \begin{pmatrix}
c_p & 0 & 0 & 0 & 0 & 0 & 0 & 0 & 0 \\
\lambda/(c_p\rho) & 0 & 0 & 0 & 0 & 0 & 0 & 0 & 0 \\
\lambda/(c_p\rho) & 0 & 0 & 0 & 0 & 0 & 0 & 0 & 0 \\
0 & 0 & 0 & c_s & 0 & 0 & 0 & 0 & 0 \\
0 & 0 & 0 & 0 & 0 & 0 & 0 & 0 & 0 \\
0 & 0 & 0 & 0 & 0 & c_s & 0 & 0 & 0 \\
0 & 0 & 0 & 0 & 0 & 0 & c_p & 0 & 0 \\
0 & 0 & 0 & 0 & 0 & 0 & 0 & c_s & 0 \\
0 & 0 & 0 & 0 & 0 & 0 & 0 & 0 & c_s
\end{pmatrix},
\tag{25}
$$

with $c_p = \sqrt{\frac{\lambda+2\mu}{\rho}}$ and $c_s = \sqrt{\frac{\mu}{\rho}}$ the P- and S-wave velocities of the unrelaxed purely elastic material.
The matrix $A^{||}$ includes the anelastic part and exhibits itself a similar block structure as in (15) of the form:

$$
A^{||} = \begin{bmatrix} A_1^{||} \\ \vdots \\ A_n^{||} \end{bmatrix} \in \mathbb{R}^{6n\times 9},
\tag{26}
$$

where each sub-matrix $A_\ell^{||} \in \mathbb{R}^{6\times 9}$, with $\ell = 1, ..., n$, contains the local unrelaxed material parameters and the relaxation frequency ω_ℓ of the ℓ-th attenuation mechanism in the form:

$$
A_\ell^{||} = \omega_\ell \cdot \begin{pmatrix}
1/(c_p\rho) & 0 & 0 & 0 & 0 & 0 & 0 & 0 & 0 \\
0 & 0 & 0 & 0 & 0 & 0 & 0 & 0 & 0 \\
0 & 0 & 0 & 0 & 0 & 0 & 0 & 0 & 0 \\
0 & 0 & 0 & 1/(2c_s\rho) & 0 & 0 & 0 & 0 & 0 \\
0 & 0 & 0 & 0 & 0 & 0 & 0 & 0 & 0 \\
0 & 0 & 0 & 0 & 0 & 1/(2c_s\rho) & 0 & 0 & 0
\end{pmatrix}.
\tag{27}
$$

Skipping the index j for the j-th face of a tetrahedral element, and recalling that the anelastic functions ϑ^ℓ are tensors like the stresses the rotation matrix $\check{T}_{pq}$ for the full anelastic system in (23) has the form

$$\check{T} = \begin{bmatrix} T^t & 0 & 0 \\ 0 & T^v & 0 \\ 0 & 0 & T_a \end{bmatrix} \in \mathbb{R}^{n_v \times n_v}, \tag{28}$$

where $T^t \in \mathbb{R}^{6\times 6}$ is the rotation matrix responsible for the stress tensor rotation as in the purely elastic part and is given as

$$T^t = \begin{pmatrix} n_x^2 & s_x^2 & t_x^2 & 2n_x s_x & 2s_x t_x & 2n_x t_x \\ n_y^2 & s_y^2 & t_y^2 & 2n_y s_y & 2s_y t_y & 2n_y t_y \\ n_z^2 & s_z^2 & t_z^2 & 2n_z s_z & 2s_z t_z & 2n_z t_z \\ n_y n_x & s_y s_x & t_y t_x & n_y s_x + n_x s_y & s_y t_x + s_x t_y & n_y t_x + n_x t_y \\ n_z n_y & s_z s_y & t_z t_y & n_z s_y + n_y s_z & s_z t_y + s_y t_z & n_z t_y + n_y t_z \\ n_z n_x & s_z s_x & t_z t_x & n_z s_x + n_x s_z & s_z t_x + s_x t_z & n_z t_x + n_x t_z \end{pmatrix}, \tag{29}$$

with the components of the normal vector $\vec{n} = (n_x, n_y, n_z)^T$ and the two tangential vectors $\vec{s} = (s_x, s_y, s_z)^T$ and $\vec{t} = (t_x, t_y, t_z)^T$, which lie in the plane determined by the boundary face of the tetrahedron and are orthogonal to each other and the normal vector $\vec{n}$ as shown in (Dumbser & Käser 2006).
The matrix $T^v \in \mathbb{R}^{3\times 3}$ is the rotation matrix responsible for the velocity vector rotation as in the purely elastic part and is given as

$$T^v = \begin{pmatrix} n_x & s_x & t_x \\ n_y & s_y & t_y \\ n_z & s_z & t_z \end{pmatrix}. \tag{30}$$

The matrix T_a in (28) is a block diagonal matrix and has the structure

$$T_a = \begin{bmatrix} T^t & & 0 \\ & \ddots & \\ 0 & & T^t \end{bmatrix} \in \mathbb{R}^{6n\times 6n}, \tag{31}$$

where each of the n sub-matrices T^t is the tensor rotation matrix given in (29).
Using the symmetries of $\check{A}$, $|\check{A}|$ and $\check{T}$ and the particular composition of the source term matrix $\check{E}$ as given in (19)- (22), we can separate the full system in (13) into two parts. We call the first 9 equations the *elastic part* and the remaining equations 10 to n_v the *anelastic part*. Therefore, the fluxes and volume integrals appearing in the discrete formulation of the Discontinuous Galerkin approach in (23) can be computed separately for each part. However, both parts are still coupled via the Cauchy-Kovalewski procedure of the ADER time integration approach and the source terms $\check{E}$ in (13).
In the following Section 3.1 we outline in detail, how this coupling is accomplished with a new, more efficient time integration approach in order to replace the costly multiplication with the four-dimensional tensor $I_{qlmn}(\Delta t)$ in (23).

3.1 The ADER Time Discretization

As in (Käser & Dumbser 2006; Dumbser & Käser 2006) we first write the governing PDE (13) in the reference system as

$$\frac{\partial Q_p}{\partial t} + \check{A}^*_{pq}\frac{\partial Q_q}{\partial \xi} + \check{B}^*_{pq}\frac{\partial Q_q}{\partial \eta} + \check{C}^*_{pq}\frac{\partial Q_q}{\partial \zeta} - \check{E}_{pq}\, Q_q = 0, \tag{32}$$

with

$$\check{A}^*_{pq} = \check{A}_{pq}\frac{\partial \xi}{\partial x} + \check{B}_{pq}\frac{\partial \xi}{\partial y} + \check{C}_{pq}\frac{\partial \xi}{\partial z}, \tag{33}$$

$$\check{B}^*_{pq} = \check{A}_{pq}\frac{\partial \eta}{\partial x} + \check{B}_{pq}\frac{\partial \eta}{\partial y} + \check{C}_{pq}\frac{\partial \eta}{\partial z}, \tag{34}$$

$$\check{C}^*_{pq} = \check{A}_{pq}\frac{\partial \zeta}{\partial x} + \check{B}_{pq}\frac{\partial \zeta}{\partial y} + \check{C}_{pq}\frac{\partial \zeta}{\partial z}. \tag{35}$$

We then develop the solution of (32) within one time step into a Taylor series in time up to order N,

$$Q_p(\xi,\eta,\zeta,t) = \sum_{k=0}^{N} \frac{(t-t^n)^k}{k!}\frac{\partial^k}{\partial t^k} Q_p(\xi,\eta,\zeta,t^n), \tag{36}$$

which we project onto each basis function in order to get an approximation of the evolution of the degrees of freedom during one time step from time level n to time level $n+1$. We obtain

$$\hat{Q}_{pl}(t) = \frac{\left\langle \Phi_n, \sum\limits_{k=0}^{N} \frac{(t-t^n)^k}{k!}\frac{\partial^k}{\partial t^k} Q_p(\xi,\eta,\zeta,t^n) \right\rangle}{\langle \Phi_n, \Phi_l \rangle}, \tag{37}$$

where $\langle a,b\rangle = \int\limits_{\mathcal{T}_E} a\cdot b\, dV$ denotes the inner product over the reference tetrahedron $\mathcal{T}_E$ and the division by $\langle \Phi_n,\Phi_l\rangle$ denotes the multiplication with the inverse of the mass matrix. This reduces indeed to division by its diagonal entries since the mass matrix is diagonal due to the supposed orthogonality of the basis functions Φ_l.

The k-th time derivative of the entire state vector Q_p is obtained via the Cauchy-Kovalewski procedure applied to the governing equation (13) in the reference system (32), and reads as

$$\frac{\partial^k}{\partial t^k}Q_p = \left(\check{A}^*_{pq}\frac{\partial}{\partial\xi} + \check{B}^*_{pq}\frac{\partial}{\partial\eta} + \check{C}^*_{pq}\frac{\partial}{\partial\zeta} - \check{E}_{pq}\right)^k Q_q\,, \tag{38}$$

which can be proven by complete induction. One could use a similar algorithm as presented in (Käser & Dumbser 2006; Dumbser & Käser 2006) to compute the Cauchy-Kovalewski procedure explicitly using the tensor $I_{plqm}\left(\Delta t\right)$, but for a possibly huge system (13) due to a large number of attenuation mechanisms, this approach turned out to be too slow. Therefore, we use an unrolled recursive procedure in order to do the Cauchy-Kovalewski procedure, similar as proposed in (Dumbser & Munz 2005c) for the nonlinear case. The unrolled recursive algorithm described in the following becomes especially efficient because the matrices $\check{A}_{pq}$, $\check{B}_{pq}$, $\check{C}_{pq}$ and $\check{E}_{pq}$ are sparse as shown in Section 3.

From (38) we deduce that the k-th time derivative depends on all mixed space derivatives up to order k. We therefore write formally

$$\frac{\partial^k}{\partial t^k}Q_p = \mathcal{C}^k_p\left(\frac{\partial^\nu}{\partial\xi^\alpha\partial\eta^\beta\partial\zeta^\gamma}Q_q\right), \qquad \forall\,(\alpha+\beta+\gamma)=\nu\le k, \tag{39}$$

insisting on the fact that the operator $\mathcal{C}^k_p$ is linear. We then insert (39) into (37) and obtain after integration over the time interval $\Delta t = t^{n+1}-t^n$

$$\tilde{Q}_{pl}(\Delta t) = \int\limits_{t=t^n}^{t^n+\Delta t}\hat{Q}_{pl}(t)dt = \frac{\left\langle \Phi_n, \sum\limits_{k=0}^{N}\frac{\Delta t^{k+1}}{(k+1)!}\mathcal{C}^k_p\left(\frac{\partial^\nu}{\partial\xi^\alpha\partial\eta^\beta\partial\zeta^\gamma}Q_q(\xi,\eta,\zeta,t^n)\right)\right\rangle}{\langle\Phi_n,\Phi_l\rangle}. \tag{40}$$

Making use of the linearity of $\mathcal{C}^k_p$ in (39) and inserting the Discontinuous Galerkin approximation for Q_p in terms of the basis functions Φ as given in (Käser & Dumbser 2006; Dumbser & Käser 2006) yields

$$\tilde{Q}_{pl}(\Delta t) = \sum_{k=0}^{N}\frac{\Delta t^{k+1}}{(k+1)!}\mathcal{C}^k_p\left(\frac{\left\langle\Phi_n,\frac{\partial^\nu}{\partial\xi^\alpha\partial\eta^\beta\partial\zeta^\gamma}\Phi_m(\xi,\eta,\zeta)\right\rangle}{\langle\Phi_n,\Phi_l\rangle}\hat{Q}_{qm}(t^n)\right), \tag{41}$$

where the operator $\mathcal{C}^k_p$ is applied to each degree of freedom l. We note that the inner products appearing in (41) are computed in the reference system, they do not depend on the mesh and therefore need to be computed only once.
Instead of using the tensor $I_{plqm}\left(\Delta t\right)$ in (23) as suggested in (Käser & Dumbser 2006; Dumbser & Käser 2006), we can now substitute this tensor in (23) by

$$I_{plmn}(\Delta t)\left(\hat{Q}^{(m)}_{mn}\right)^n := \tilde{Q}^{(m)}_{pl}(\Delta t)\,. \tag{42}$$

The operator $\mathcal{C}^k_p$ from (39) is defined recursively as

$$\begin{aligned}\frac{\partial^{k+1+\alpha+\beta+\gamma}}{\partial t^{k+1}\partial\xi^\alpha\partial\eta^\beta\partial\zeta^\gamma}Q_q \;=\;& -\check{A}^*_{pq}\frac{\partial^{k+\alpha+1+\beta+\gamma}}{\partial t^k\partial\xi^{\alpha+1}\partial\eta^\beta\partial\zeta^\gamma}Q_q - \check{B}^*_{pq}\frac{\partial^{k+\alpha+\beta+1+\gamma}}{\partial t^k\partial\xi^\alpha\partial\eta^{\beta+1}\partial\zeta^\gamma}Q_q\\ & -\check{C}^*_{pq}\frac{\partial^{k+\alpha+\beta+\gamma+1}}{\partial t^k\partial\xi^\alpha\partial\eta^\beta\partial\zeta^{\gamma+1}}Q_q - \left(-\check{E}_{pq}\right)\frac{\partial^{k+\alpha+\beta+\gamma}}{\partial t^k\partial\xi^\alpha\partial\eta^\beta\partial\zeta^\gamma}Q_q\,.\end{aligned} \tag{43}$$

To clarify the procedure of the high-order ADER time integration, a FORTRAN code for implementing $\mathcal{C}^k_p$ in an unrolled recursive manner making use of the sparsity of the system matrices may e.g. look like the example presented in Table 1. The ordering of the dimensions of the array W appearing in this code is as follows: (1) projections onto all test functions, (2) variables of the hyperbolic system, (3) ξ derivatives, (4) η derivatives, (5) ζ derivatives and (6) time derivatives. We note that in the example code in Table 1 the subarray $W(:,:,:,:,:,0)$ contains the projections of all space derivatives onto each test function, which is precisely the argument of the operator $\mathcal{C}^k_p$ in (41). The final result of the operator, i.e. all time-derivatives of all degrees of freedom, is contained in the sub-array $W(:,:,0,0,0,:)$. The other entries of W contain intermediate results (mixed space-time derivatives) which are produced by the algorithm.

Table 1. Fortran example code of the unrolled recursive algorithm for the Cauchy-Kovalewski procedure using the sparsity of the system matrices.

```
TYPE tSparseMatrix                                                          ! Type, defining a sparse matrix
  INTEGER :: n                                                              ! Dimension of the original matrix
  INTEGER, POINTER :: nNonZero                                              ! Number of non-zero entries
  INTEGER, POINTER :: NonZeroIndex1(:)                                      ! Row indices of non-zero elements
  INTEGER, POINTER :: NonZeroIndex2(:)                                      ! Column indices of non-zero elements
  REAL, POINTER :: NonZero(:)                                               ! Non-zero values
END TYPE tSparseMatrix                                                      !
!                                                                           !
! Subroutine doing the CK Procedure for the linear system with source term: !
! u_t + Au_x + Bu_y + Cu_z = -(-E) u                                        !
!                                                                           !
SUBROUTINE CauchyKovalewski_Sparse_Linear(nDegFr,nVar,N,W,A,B,C,E)          !
  IMPLICIT NONE                                                             !
  ! Argument list declaration                                               !
  INTEGER :: N                                                              ! Polynomial order N of the basis functions
  INTEGER :: nDegFr                                                         ! Number of degrees of freedom (DOF) per element
  INTEGER :: nVar                                                           ! Number of variables n_v of the hyperbolic system
  TYPE(tSparseMatrix) :: A,B,C,E                                            ! Sparse system matrices Ǎ*_pq, B̌*_pq, Č*_pq, -Ě_pq
  ! Local Variables                                                         !
  REAL :: W(nDegFr,nVar,0:N,0:N,0:N,0:N)                                    ! Array of space-time derivatives for all DOF and all variables
  REAL :: Tmp(nDegFr,nVar)                                                  ! Temporary vector
  INTEGER :: k,alpha,beta,gamma                                             ! Loop counters for t, ξ, η, ζ derivatives
  INTENT(IN) :: nDegFr,nVar,N, A, B, C, E                                   ! Intent definition for the arguments
  INTENT(INOUT) :: W                                                        ! W(:,:,:,:,:,0) enters with pure space derivatives
  !                                                                         ! and W(:,:,0,0,0,:) leaves with all time derivatives,
  !                                                                         ! i.e. with the result of the operator C_p^k for all DOF
  DO k = 0, (N-1)                                                           ! Advance forward in time
    DO alpha = 0, (N-1-k)                                                   ! Loop over all ξ derivatives
      DO beta = 0, (N-1-alpha-k)                                            ! Loop over all η derivatives
        DO gamma = 0, (N-1-alpha-beta-k)                                    ! Loop over all ζ derivatives
          Tmp(:,:) = 0.                                                     ! Initialize temporary vector
          CALL SP_MATMUL(Tmp,A,W(:,:,alpha+1,beta, gamma ,k ),nVar,nDegFr)  ! Multiply with sparse matrix Ǎ*_pq and subtract                ll
          CALL SP_MATMUL(Tmp,B,W(:,:,alpha, beta+1,gamma ,k ),nVar,nDegFr)  ! Multiply with sparse matrix B̌*_pq and subtract
          CALL SP_MATMUL(Tmp,C,W(:,:,alpha, beta, gamma+1,k ),nVar,nDegFr)  ! Multiply with sparse matrix Č*_pq and subtract
          CALL SP_MATMUL(Tmp,E,W(:,:,alpha, beta, gamma ,k ),nVar,nDegFr)   ! Multiply with sparse matrix -Ě_pq and subtract
          W(:,:,alpha,beta,gamma,k+1) = Tmp(:,:)                            ! Write result into W array
        ENDDO                                                               !
      ENDDO                                                                 !
    ENDDO                                                                   !
  ENDDO                                                                     !
END SUBROUTINE CauchyKovalewski_Sparse_Linear                               !
!                                                                           !
! The subroutine SP_MATMUL multiplies a sparse matrix A from the left to the transpose !
! of a full matrix B and subtracts the result from the transposed matrix C:  !
! C_ki = C_ki - A_ij * B_kj                                                  !
!                                                                           !
PURE SUBROUTINE SP_MATMUL(C, A, B, n, m)                                    !
  IMPLICIT NONE                                                             !
  ! Argument list declaration                                               !
  TYPE(tSparseMatrix) :: A                                                  ! Sparse matrix of dimension (n,n)
  INTEGER :: n,m                                                            ! Matrix dimensions n and m
  REAL :: C(m,n)                                                            ! Result matrix of dimension (m,n)
  REAL :: B(m,n)                                                            ! Full matrix of dimension (m,n)
  ! Local variable declaration                                              !
  INTEGER :: i,j,iNonZero                                                   ! Loop counters
  INTENT(IN) :: n,m,A,B                                                     ! Intent definition for the arguments
  INTENT(INOUT) :: C                                                        ! Intent definition for the arguments
  DO iNonZero = 1, A%nNonZero                                               ! Loop over all non-zero entries of A
    i = A%NonZeroIndex1(iNonZero)                                           ! Get row index
    j = A%NonZeroIndex2(iNonZero)                                           ! Get column index
    C(:,i) = C(:,i) - B(:,j)*A%NonZero(iNonZero)                            ! Multiply and subtract
  ENDDO                                                                     !
END SUBROUTINE SP_MATMUL                                                    !
```

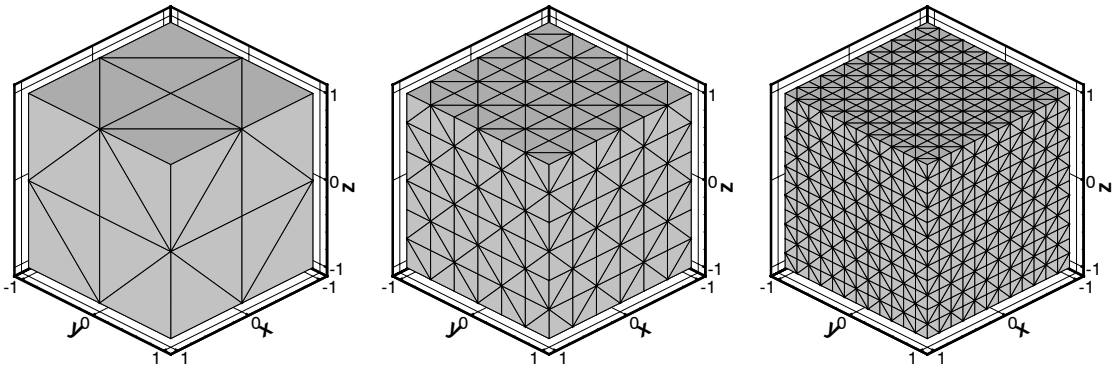

Figure 1. Sequence of discretizations of the computational domain Ω via regularly refined tetrahedral meshes, which are used for the numerical convergence analysis.

4 CONVERGENCE ANALYSIS

In this Section we present the results of a numerical convergence analysis to demonstrate the very high accuracy of the proposed ADER-DG method on tetrahedral meshes considering viscoelastic attenuation. We show results from second to seventh order ADER-DG schemes, which are denoted by ADER-DG $\mathcal{O}2$ to ADER-DG $\mathcal{O}7$ respectively. Note, that the same order for time and space accuracy is automatically obtained.

To determine the convergence orders we solve the three-dimensional seismic wave equations with viscoelastic attenuation in (12) on the unit-cube as sketched in Figure 1, i.e. on a computational domain $\Omega = [-1,1] \times [-1,1] \times [-1,1] \in \mathbb{R}^3$ with periodic boundary conditions. The homogeneous material parameters are set to

$$\lambda = 2, \qquad \mu = 1, \qquad \rho = 1, \qquad Q_P = 20, \qquad Q_S = 10, \tag{44}$$

throughout the computational domain Ω. The Q-factors are assumed to be frequency independent over the frequency band $[0.1, 10]$ Hz. To this end, we are using 5 mechanisms as outlined in Section 2 leading to approximations of frequency independent Q-factors Q_P and Q_S as shown in Figure 3. This attenuation properties introduce damping and dispersion of the P- and S-waves.

We know, e.g. from (Stein & Wysession 2003), that the analytical solution to this problem has the form

$$Q_p(x,y,z,t) = Q_p^0 \cdot e^{i\cdot(\omega t - k_x x - k_y y - k_z z)}, \qquad p = 1, ..., n_v \tag{45}$$

where Q_p^0 is the initial amplitude vector, ω the wave frequencies to determine, and

$$\vec{k} = (k_x, k_y, k_z)^T = (\pi, \pi, \pi)^T . \tag{46}$$

is the wave number leading to a periodic, plane sinusoidal wave in the unit-cube with the wave front perpendicular to the cube's space diagonal.

In the following, we briefly line out, how we determine the wave frequencies ω:

With the assumption, that equation (45) is the analytic solution of the governing equation (13), we calculate the first time and space derivatives of equation (45) analytically and plug them into equation (13). From there, we can derive the eigen-problem

$$(\check{A}_{pq} k_x + \check{B}_{pq} k_y + \check{C}_{pq} k_z - i \cdot \check{E}_{pq}) \cdot Q_q^0 = \omega \cdot Q_q^0, \qquad p, q = 1, ..., n_v. \tag{47}$$

Solving the eigenproblem (47) gives us the matrix R_{pq} of right eigenvectors $R_{p1}, ..., R_{pn_v}$ and the eigenvalues ω_p.

Recalling, e.g. from (Toro 1999), that each solution of the linear hyperbolic system (13) is given by a linear combination of the right eigenvectors, i.e. $Q_p = R_{pq}\nu_q$, we can compute the coefficients as $\nu_p = R_{pq}^{-1} Q_q^0$ via the initial amplitude vector. Now, we can synthesize the exact solution of the attenuated plane wave in the form

$$Q_p(x,y,z,t) = R_{pq} c_q \cdot e^{i\cdot(\omega_q t - k_x x - k_y y - k_z z)} . \tag{48}$$

In the convergence test, we use a plane P-wave and a plane S-wave travelling in opposite directions along the space diagonal $\vec{n} = (1,1,1)^T$ of the domain Ω as already shown in (Dumbser & Käser 2006). Therefore, the initial condition at $t = 0$ is given by (48) using the combination

Table 2. Convergence rates of velocity component v of the ADER-DG $\mathcal{O}2$ up to ADER-DG $\mathcal{O}7$ schemes on tetrahedral meshes with viscoelastic attenuation.

h	L^∞	$\mathcal{O}_{L^\infty}$	L^2	$\mathcal{O}_{L^2}$	N_d	I	CPU [s]
$1.08 \cdot 10^{-1}$	$5.8427 \cdot 10^{-3}$	–	$4.9154 \cdot 10^{-3}$	–	81920	24	54
$7.21 \cdot 10^{-2}$	$2.5832 \cdot 10^{-3}$	2.0	$2.1258 \cdot 10^{-3}$	2.0	276480	36	237
$5.41 \cdot 10^{-2}$	$1.5283 \cdot 10^{-3}$	1.8	$1.1675 \cdot 10^{-3}$	2.0	655360	46	654
$4.33 \cdot 10^{-2}$	$9.6624 \cdot 10^{-4}$	2.0	$7.4891 \cdot 10^{-4}$	2.0	1280000	58	2554
$2.16 \cdot 10^{-1}$	$5.2416 \cdot 10^{-3}$	–	$3.3154 \cdot 10^{-3}$	–	25600	20	11
$1.08 \cdot 10^{-1}$	$6.1884 \cdot 10^{-4}$	3.0	$3.4172 \cdot 10^{-4}$	3.2	204800	38	141
$7.21 \cdot 10^{-2}$	$1.6466 \cdot 10^{-4}$	3.2	$1.0371 \cdot 10^{-4}$	2.9	691200	58	667
$5.41 \cdot 10^{-2}$	$7.9007 \cdot 10^{-5}$	2.6	$4.2568 \cdot 10^{-5}$	3.0	1638400	76	1884
$2.16 \cdot 10^{-1}$	$5.4019 \cdot 10^{-4}$	–	$3.2650 \cdot 10^{-4}$	–	51200	28	38
$1.44 \cdot 10^{-1}$	$1.4035 \cdot 10^{-4}$	3.3	$5.7098 \cdot 10^{-5}$	4.3	172800	40	167
$1.08 \cdot 10^{-1}$	$4.3849 \cdot 10^{-5}$	4.0	$1.7294 \cdot 10^{-5}$	4.1	409600	54	502
$7.21 \cdot 10^{-2}$	$9.0593 \cdot 10^{-6}$	3.9	$3.2289 \cdot 10^{-6}$	4.1	1382400	80	2349
$4.33 \cdot 10^{-1}$	$1.8628 \cdot 10^{-3}$	–	$8.2639 \cdot 10^{-4}$	–	11200	18	12
$2.16 \cdot 10^{-1}$	$7.6600 \cdot 10^{-5}$	4.6	$2.2934 \cdot 10^{-5}$	5.1	89600	36	153
$1.44 \cdot 10^{-1}$	$9.2101 \cdot 10^{-6}$	5.2	$2.8075 \cdot 10^{-6}$	5.1	302400	52	707
$1.08 \cdot 10^{-1}$	$2.4793 \cdot 10^{-6}$	4.6	$6.5511 \cdot 10^{-7}$	5.0	716800	70	2141
$8.66 \cdot 10^{-1}$	$2.3332 \cdot 10^{-2}$	–	$5.5446 \cdot 10^{-3}$	–	2240	12	5
$4.33 \cdot 10^{-1}$	$3.5278 \cdot 10^{-4}$	6.0	$9.2971 \cdot 10^{-5}$	5.8	17920	22	43
$2.16 \cdot 10^{-1}$	$6.4411 \cdot 10^{-6}$	5.8	$1.3848 \cdot 10^{-6}$	6.0	143360	42	537
$1.44 \cdot 10^{-1}$	$5.8832 \cdot 10^{-7}$	5.9	$1.1679 \cdot 10^{-7}$	6.0	483840	64	2645
$8.66 \cdot 10^{-1}$	$4.4462 \cdot 10^{-3}$	–	$1.3201 \cdot 10^{-3}$	–	3360	14	15
$4.33 \cdot 10^{-1}$	$4.8205 \cdot 10^{-5}$	6.5	$1.2198 \cdot 10^{-5}$	6.7	26880	26	133
$2.88 \cdot 10^{-1}$	$3.3500 \cdot 10^{-6}$	6.6	$5.8371 \cdot 10^{-7}$	7.4	90720	38	581
$2.16 \cdot 10^{-1}$	$4.4073 \cdot 10^{-7}$	7.0	$7.6456 \cdot 10^{-8}$	7.0	215040	50	1694

of only two right eigenvectors $(R_{p2}, ..., R_{p9})$ with the coefficients $\nu_2 = \nu_9 = 1$ and zero otherwise.
The total simulation time T is set to $T = 0.1$s. The CFL number is set in all computations to 50% of the stability limit $\frac{1}{2N+1}$ of Runge-Kutta DG schemes. For a thorough investigation of the linear stability properties of the ADER-DG schemes via a von Neumann analysis see (Dumbser 2005).
The numerical analysis to determine the convergence orders is performed on a sequence of tetrahedral meshes as shown in Figure 1. The mesh sequence is obtained by dividing the computational domain Ω into a number of subcubes, which are then subdivided into five tetrahedrons as shown in Figure 1. This way, the refinement is controlled by changing the number of subcubes in each space dimension.
We can arbitrarily pick one of the variables of the system of the seismic wave equations (13) to numerically determine the convergence order of the used ADER-DG schemes. In Table 2 we show the errors for the shear stress component σ_{yz}. The errors of the numerical solution Q_h with respect to the exact solution Q_e is measured in the L^∞-norm and the continuous L^2-norm

$$\|Q_h - Q_e\|_{L^2(\Omega)} = \Big(\int_\Omega |Q_h - Q_e|^2 \, dV \Big)^{\frac{1}{2}}, \tag{49}$$

where the integration is approximated by Gaussian integration which is exact for a polynomial degree twice that of the basis functions of the numerical scheme. The L^∞-norm is approximated by the maximum error arising at any of these Gaussian integration points. The first column in Table 2 shows the mesh spacing h, represented by the maximum diameter of the circumscribed spheres of the tetrahedrons. The following four columns show the L^∞ and L^2 errors with the corresponding convergence orders $\mathcal{O}_{L^\infty}$ and $\mathcal{O}_{L^2}$ determined by successively refined meshes. Furthermore, we present the total number N_d of degrees of freedom, which is a measure of required storage space during run-time and is given through the product of the number of total mesh elements and the number N_e of degrees of freedom per element. N_e depends on the order of the scheme, i.e. the degree N of the polynomial basis functions via $N_e(N) = \frac{1}{6}(N+1)(N+2)(N+3)$. In the last two columns we give the number I of iterations and the CPU times in seconds needed to reach the simulation time $T = 0.1$s on a Pentium Xeon 3.6 GHz processor with 4GB of RAM.

In Figure 2 we visualize the convergence results of Table 2 to demonstrate the dependence of the L^∞ error with respect to (a) mesh width h, (b) number of degrees of freedom N_d and (c) CPU. We remark, that in all three plots of Figure 2 we clearly show, that for very high accuracy, the higher order schemes pay of due to their convergence properties.
In the following, we investigate the accuracy of the approximation of a given, generally constant $\mathcal{Q}$-law with respect to the number of attenuation mechanisms as described in Section 2.

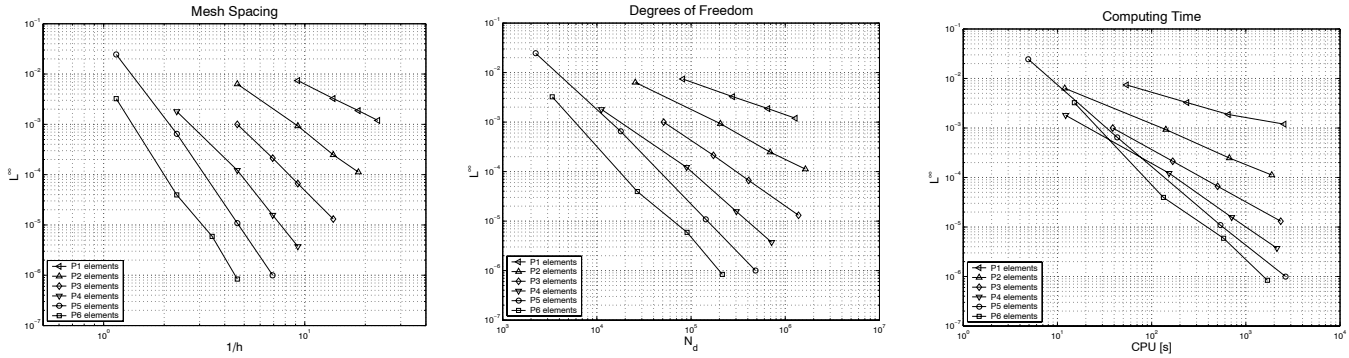

(a) (b) (c)

Figure 2. Convergence rates of velocity component v of Table 2. The L^∞ error is plotted versus (a) the mesh spacing h, (b) the number of degrees of freedom N_d and (c) the CPU time.

[

Table 3. Computational effort with increasing number of mechanisms of the ADER-DG $\mathcal{O}2$ up to ADER-DG $\mathcal{O}6$ schemes.

n	0	1	2	3	4	5	6	7	8	9	10
$\mathcal{O}2$	1.00	1.38	1.48	1.62	1.68	1.82	1.88	1.95	2.08	2.18	2.27
$\mathcal{O}3$	1.00	1.49	1.70	1.91	2.07	2.28	2.49	2.66	2.82	2.99	3.20
$\mathcal{O}4$	1.00	1.77	2.07	2.43	2.70	2.99	3.34	3.69	4.03	4.47	4.67
$\mathcal{O}5$	1.00	1.92	2.30	2.83	3.27	3.84	4.38	4.83	5.40	5.77	6.32
$\mathcal{O}6$	1.00	1.93	2.44	3.00	3.55	4.13	4.65	5.06	5.82	6.44	6.87

5 QUALITY FACTOR APPROXIMATION

We demonstrate the improvement of the approximation of a frequency-independent $\mathcal{Q}$-law as recognized in the work of (Liu, Anderson & Kanamori 1976) when increasing the number n of attenuation mechanisms. Furthermore, we analyse the corresponding, additional CPU time requirements, when different orders of accuracy of the ADER-DG schemes are used in combination with an increasing number of such mechanisms.

Figure 3 shows, how a constant $\mathcal{Q}$-law can be fitted by using (a) 2, (b) 3, (c) 5 or (d) 10 attenuation mechanisms on a frequency band of $[0.1, 10]$Hz. We point out, that following the lines in (Emmerich & Korn 1987) already 3 attenuation mechanisms approximate a constant, frequency-independent $\mathcal{Q}$-law with a maximum derivation of around 5%. Using only 2 attenuation mechanisms seems to be a too rough approximation whereas 5 or more mechanisms already lead to a $\mathcal{Q}$-law approximations which might not even be necessary in most cases. The influence of the number of used attenuation mechanisms on seismograms recorded for an anelastic subsurface model is studied in Section 6. Table 3 shows the increasing CPU time, when the number n of mechanisms is increased. The CPU times are normalized with respect to the purely elastic case, where no attenuation is incorporated, i.e. $n = 0$. We remark, that 3 mechanisms, as typically suggested in the literature e.g. by Emmerich & Korn (1987) or Moczo *et al.* (1997), only increase the computational effort between a factor of 1.6 and 3.0 depending on the order of the used ADER-DG scheme. This efficiency is quite remarkable, in particular, as we treat the anelastic functions, i.e. the anelastic part of (13) as described in 3, with the same (full) order of accuracy.

6 APPLICATION EXAMPLE

We apply the proposed ADER-DG method on a well-defined three-dimensional test problem, which was published in the final report of the *LIFELINES PROGRAM TASK* $1A02$ (Day, Bielak, Dreger, Graves, Larsen, Olsen & Pitarka 2003) of the Pacific Earthquake Engineering Research Center. The test case is part of a multi-institutional code validation project of a series of different numerical methods employed in numerical modelling of earthquake ground motion in three-dimensional earth models. Therefore, besides a quasi-analytic solution, simulation results from four different well-established codes exist and serve as additional reference solutions. The results of these four codes are denoted by four-character abbreviations indicating the respective institutions:
UCBL (Doug Dreger and Shawn Larsen, University of California, Berkeley/Lawrence Livermore National Laboratory),
UCSB (Kim Olsen, University of California, Santa Barbara),
WCC2 (Arben Pitarka, URS Corporation), and
CMUN (Jacobo Bielak, Carnegie-Mellon University).

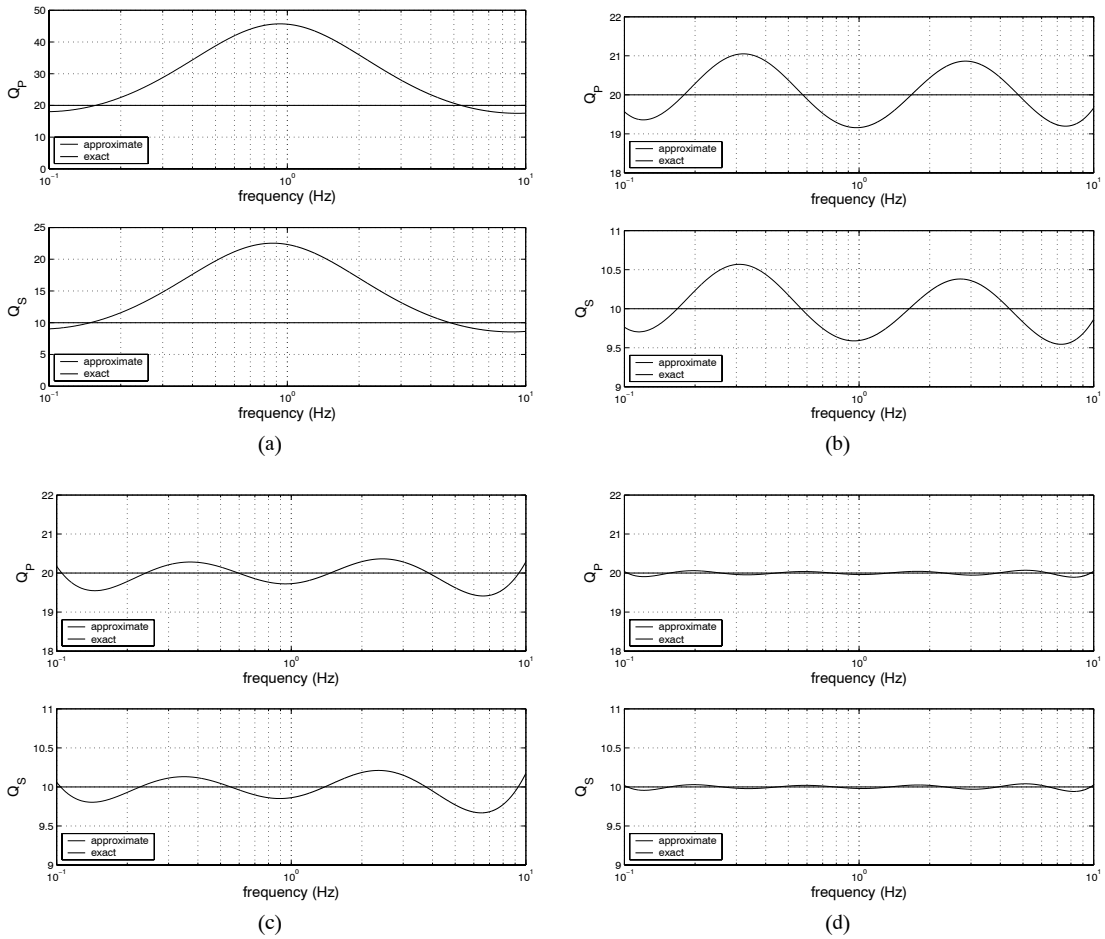

Figure 3. Approximation of frequency independent Q-factors using (a) 2, (b) 3, (c) 5 or (d) 10 mechanisms on a frequency band of $[0.1, 10]$Hz.

The first three codes use Finite Differences of uniform, structured grids with staggered locations of the velocity and stress components and fourth order accuracy in space. The CMUN code uses piecewise linear interpolation on unstructured tetrahedral Finite Elements.

The quasi-analytic solution is a frequency-wavenumber solution obtained by a modification of the method presented in (Luco & Apsel 1983; Apsel & Luco 1983) and is compared to all numerical solutions to evaluate their accuracy. The setup of the test problem LOH.3 (Layer Over Halfspace) is shown in Figure 4(a), where for clarity only one of four symmetrical quarters of the complete computational domain $\Omega = [-15000m, 15000m] \times [-15000m, 15000m] \times [0m, 17000m]$ is plotted. The material parameters of the attenuating layer (Medium 1) of the top $1000m$ over the attenuating halfspace (Medium 2) are given in Table 4.

The seismic source is a point dislocation, represented by a double couple source, where the only non-zero entries of the seismic moment tensor are $M_{xy} = M_{yx} = M_0 = 10^{18} Nm$. The location of the point source is $(x_s, y_s, z_s) = (0m, 0m, 2000m)$, i.e. in the center of the xy plane of the domain Ω in $2000m$ depth.

The moment-rate time history is given through the source time function

$$S^T(t) = \frac{t}{T^2} \exp(-\frac{t}{T}), \tag{50}$$

where the smoothness parameter T, controlling the frequency content and amplitude of the source time function, is set to $T = 0.1$s. We remark, that details of the discretization of external source terms in the framework of ADER-DG methods are outlined in previous work (Käser & Dumbser 2006).

The signals are recorded up to a simulation time of 9s by 10 receivers on the free surface as indicated in Figure 4(a). The receiver locations $(x_i, y_i, z_i) = (i \cdot 600m, i \cdot 800m, 0m)$, for $i = 1, ..., 10$.

The computational domain Ω is discretized by an unstructured, tetrahedral mesh as shown in Figure 4(b) using 249338 elements. Furthermore, the mesh is generated in a problem-adapted manner. To this end, in the zone of interest the waves traveling from the source to the receivers pass through tetrahedral elements with an average edge length of 350m, whereas in other zones the mesh is coarsened up to average edge lengths of 3000m to reduce the number of total elements and therefore computational cost. We remark that neither the source location nor the receiver locations have to coincide with nodes of the tetrahedral mesh, as in the ADER-DG framework the numerical solution is represented by polynomials within each element and therefore can be evaluated at any position within an element (see (Käser & Dumbser 2006)). This greatly simplifies the process of mesh generation and does not restrict the desired flexibility provided by unstructured meshes. However, the

Table 4. Material parameters for the LOH.3 test case. Note, that attenuation will cause dispersion of the P- and S-waves such that the given wave speeds refer to a reference frequency $f_r = 2.5$Hz.

	$c_p(f_r)[m/s]$	$c_s(f_r)[m/s]$	$\rho[kg/m^3]$	$\lambda(f_r)[GPa]$	$\mu(f_r)[GPa]$	Q_p	Q_s
Medium 1	4000	2000	2600	20.8	10.4	120	40
Medium 2	6000	3464	2700	32.4	32.4	155.9	69.3

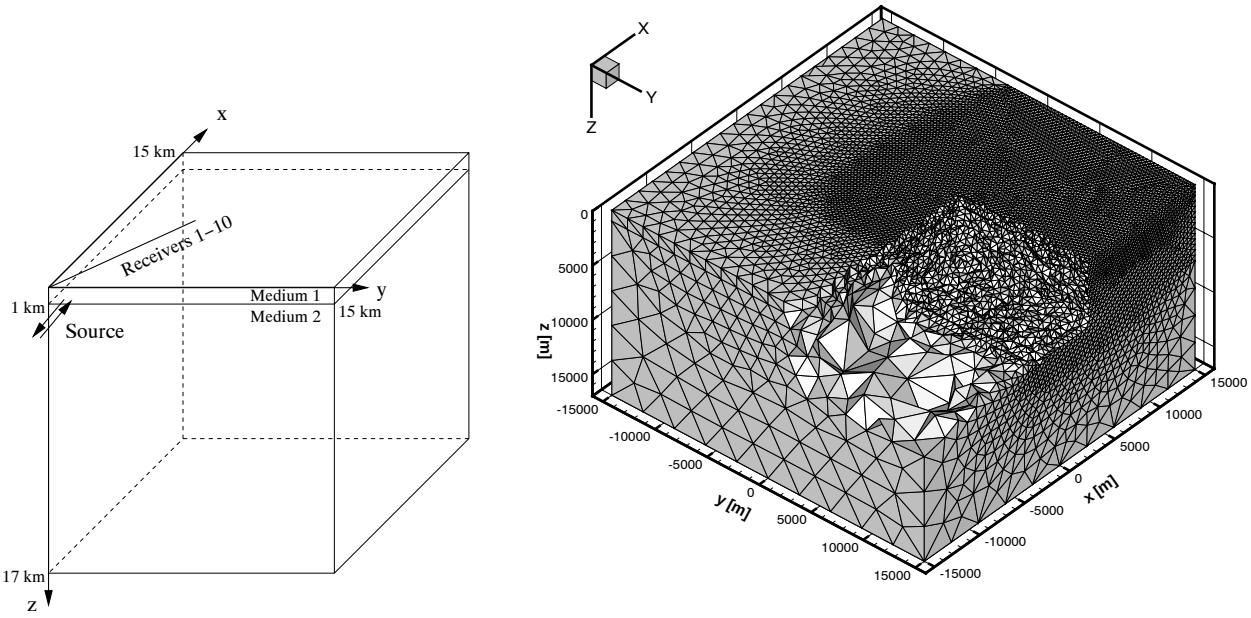

(a) (b)

Figure 4. (a) One of four symmetric quarters is shown for the LOH.3 test case, where a layer of 1km (Material 1) is lying on top of another layer (Material 2). The source is a point dislocation at $2000km$ depth represented by a moment tensor with the only non-zero components $M_{xy} = M_{yx}$. (b) Cut into the discretization of the LOH.3 model to visualize the problem-adapted tetrahedral mesh, which is refined in the quarter under the receiver line to a depth of $6000m$.

mesh respects the material interface between Medium 1 and Medium 2 as the faces of the tetrahedral elements are aligned with the material interface as shown in Figure 4(a) and (b).

In the following, we present the comparison of our results obtained by an ADER-DG $\mathcal{O}4$ and ADER-DG $\mathcal{O}5$ scheme and the four results of the reference codes (UCBL, UCSB, WCC2 and CMUN) against the analytical solution. Analogous to the LOH.3 test case in the *LIFELINES PROGRAM TASK* $1A02$ the visual comparisons in Figure 5 show the radial, transversal and vertical components of the seismic velocity field recorded at receiver 10 at $(x_{10}, y_{10}, z_{10}) = (6000m, 8000m, 0m)$. Additionally, each plot gives the relative seismogram misfit

$$E = \sum_{j=1}^{n_t} (s_j - s_j^a)^2 / \sum_{j=1}^{n_t} (s_j^a)^2, \tag{51}$$

where n_t is number of time samples of the seismogram, s_j is the numerical value of the particular seismogram at sample j and s_j^a is the corresponding analytical value. We remark, that for all shown seismograms, the original source was deconvolved and replaced by a Gaussian of spread 0.05 as described in (Day, Bielak, Dreger, Graves, Larsen, Olsen & Pitarka 2003).

The four reference solutions shown in Figure 5(a)-(d) remarkably differ from each other due to the different ways of incorporating viscoelastic attenuation. Amplitude errors (e.g. for CMUN) and phase errors (e.g. for UCSB) are quite noticeable. In addition, the results of UCBL, WCC2 and CMUN produce strong, unphysical oscillations in the transverse component.
The results with the fourth-order ADER-DG $\mathcal{O}4$ scheme in Figure 5(e) using 3 attenuation mechanisms clearly match the analytic solution better and show lower numbers for the misfit E. Furthermore, the appearing but rather small errors can even be dramatically decreased by using the higher order ADER-DG $\mathcal{O}5$ scheme in Figure 5(f). As seen also in the convergence results of Table 2, the ADER-DG $\mathcal{O}5$ simulation took about four time longer than the ADER-DG $\mathcal{O}4$. Unfortunately, run times for the reference solutions are neither given in the

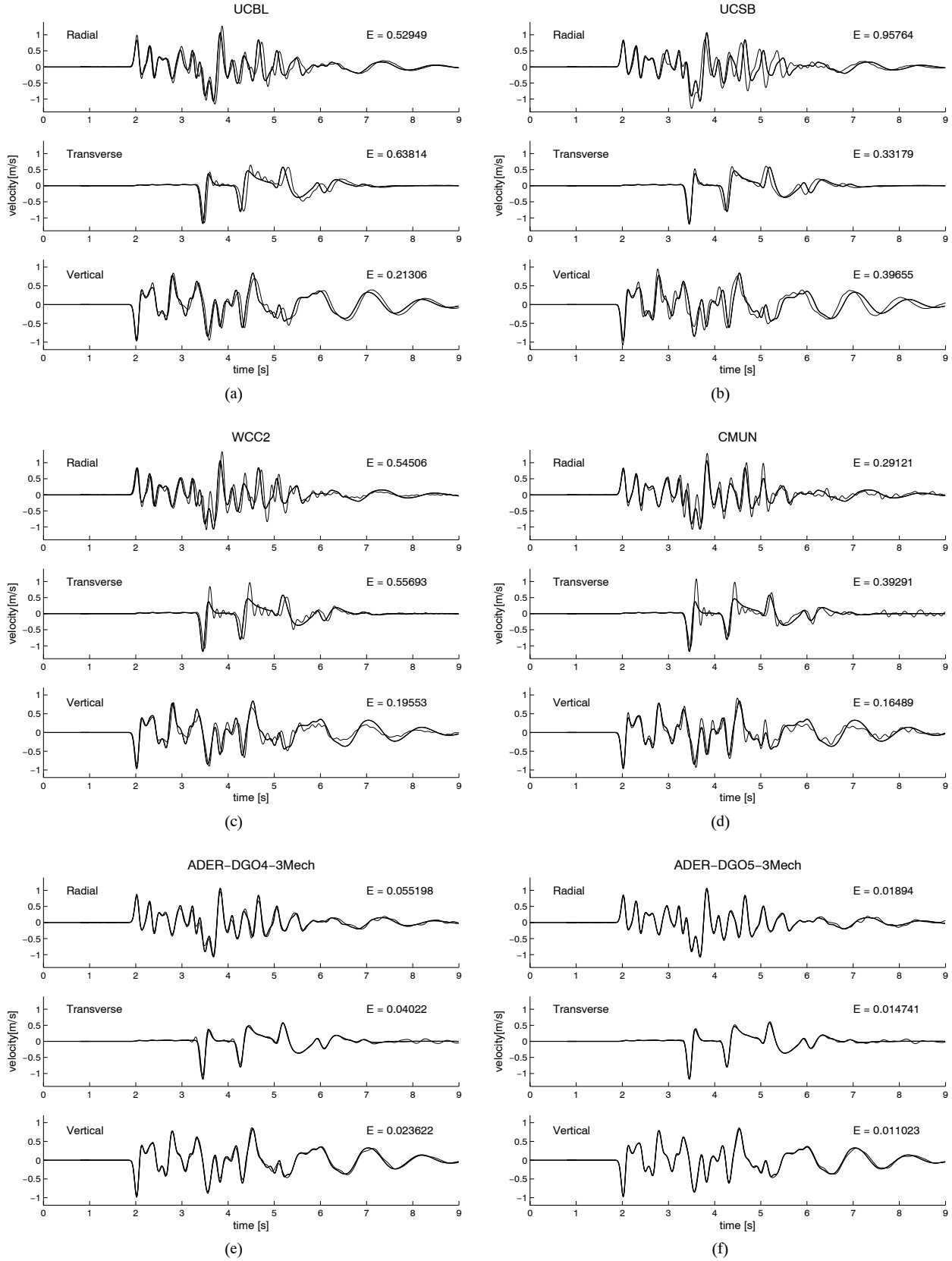

Figure 5. Comparison of the radial, transverse and vertical velocity components for the LOH.3 test case on receiver 10. The analytical solution (thick line) is plotted against the numerical one (thin line) obtained by (a) UCBL, (b) UCSB, (c) WCC2, (d) CMUN, (e) ADER-DG $\mathcal{O}4$ with 3 attenuation mechanisms and (f) ADER-DG $\mathcal{O}5$ with 3 attenuation mechanisms. The relative seismogram misfit E from equation (51) is given for each trace.

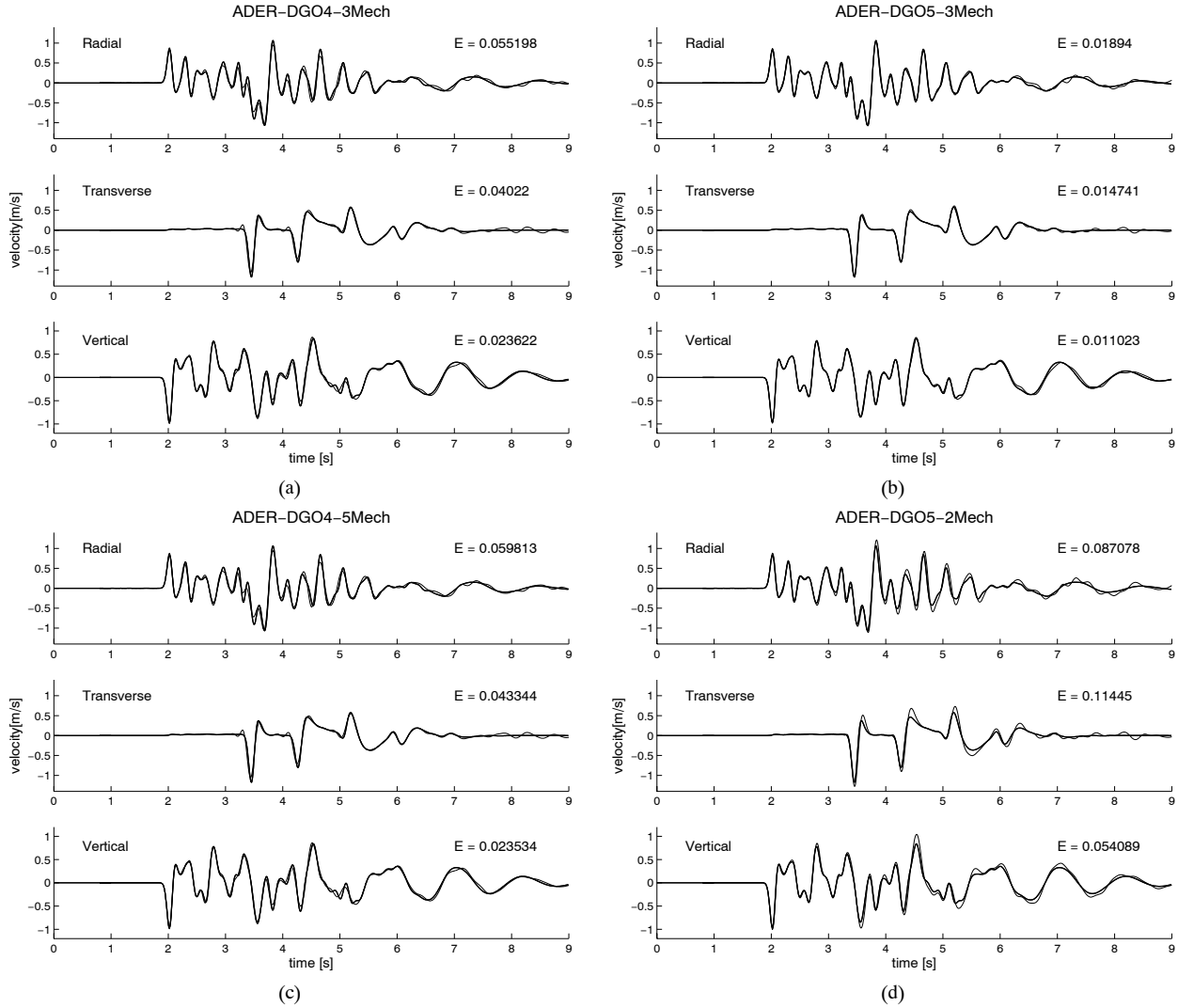

Figure 6. Comparison of the radial, transverse and vertical velocity components for the LOH.3 test case on receiver 10. The analytical solution (thick line) is plotted against the numerical one (thin line) obtained by (a) ADER-DG $\mathcal{O}4$ with 3 attenuation mechanisms, (b) ADER-DG $\mathcal{O}5$ with 3 attenuation mechanisms, (c) ADER-DG $\mathcal{O}4$ with 5 attenuation mechanisms and (d) ADER-DG $\mathcal{O}5$ with 2 attenuation mechanisms. The relative seismogram misfit E from equation (51) is given for each trace.

report of (Day, Bielak, Dreger, Graves, Larsen, Olsen & Pitarka 2003) nor could they be found elsewhere. We also remark, that the weak oscillations after 6sec in our results might be due to reflections from the model boundaries as we are not using sophisticated conditions for absorbing, non-reflecting boundaries but control them via fluxes as described in detail in (Käser & Dumbser 2006; Dumbser & Käser 2006). Figure 6(a)-(d) presents the influence of the number of attenuation mechanisms on the seismograms. Using an ADER-DG $\mathcal{O}4$ scheme with 3 or 5 mechanisms basically does not affect the seismogram accuracy as shown in Figure 6(a) and (c). Therefore, 3 mechanisms already seem to approximate the constant $\mathcal{Q}$-law with sufficient accuracy, which agrees with observations made in the literature, e.g. in (Emmerich & Korn 1987; Moczo, Bystricky, Kristek, Carcione & Bouchon 1997). However, results of the ADER-DG $\mathcal{O}5$ schemes with 2 or 3 mechanisms in Figure 6(b) and (d) clearly demonstrate that 2 mechanisms do not accurately represent a constant $\mathcal{Q}$-law as already mentioned in Section 5. Hereby we confirm, that amplitude and phase errors visible in Figure 6(d) have to be due to the insufficient $\mathcal{Q}$-law approximation instead of lacking accuracy of the numerical scheme itself. Therefore, we claim that in general 3 attenuation mechanisms might be enough to incorporate viscoelastic attenuation in many cases.

7 CONCLUSION

We have presented the incorporation of realistic attenuation of seismic waves into the new ADER-Discontinuous Galerkin (ADER-DG) schemes using viscoelastic material. The proposed numerical method can approximate the seismic wave field, i.e. stresses and velocities, with arbitrarily high order of accuracy in space and time on unstructured three-dimensional tetrahedral meshes. The additional variables, the

anelastic functions, can be treated similarly in the case of viscoelastic material. Therefore, the linear hyperbolic system of the seismic wave equations increases with the number of attenuation mechanisms and includes source terms resulting from the approximating viscoelastic material behaviour by a generalized Maxwell body. However, the introduction of a new Cauchy-Kovalewski procedure for the high order ADER time integration results in a more efficient implementation and therefore does not increase the computation time dramatically when incorporating viscoelastic attenuation. The convergence results demonstrate the high accuracy of the ADER-DG schemes on tetrahedral meshes. In addition, the detailed investigation of the required number of attenuation mechanisms agrees with the suggestions in the literature, that 3 mechanisms seem to be sufficient for the accurate incorporation of realistic attenuation. The solution of a well-established benchmark test with different orders of accuracy of the ADER-DG schemes and the comparison of the obtained results against analytic solutions clearly shows the dramatic increase in accuracy with respect to reference solutions obtained by other methods. Therefore, the proposed ADER-DG methods represents a new numerical scheme simulating seismic wave propagation with unforeseen accuracy on unstructured three-dimensional tetrahedral meshes thoroughly including realistic attenuation due to viscoelasticity.

ACKNOWLEDGMENT

The work was supported by the DFG (Deutsche Forschungsgemeinschaft) through the Emmy Noether-program (KA 2281/1-1) and the DFG-CNRS research group FOR 508, Noise Generation in Turbulent Flows and by the European Research and Training Network SPICE (Seismic Wave Propagation in Complex Media: a European Network). The support and comments by Steven Day to set up the LOH.3 test case and providing the analytical and reference solutions are highly acknowledged. We also thank Peter Moczo and Geza Seriani for the helpful support when incorporate viscoelastic attenuation. The support of the super-computing facilities of the HLRS in Stuttgart and the LRZ in München are highly appreciated for performing the calculations presented in this article.

REFERENCES

Apsel, R.J. & Luco, J.E., 1983. On the Greens functions for a layered half-space, Part II, *Bull. Seism. Soc. Am.*, **73**, 931951.

Bouchon, M., 1981. A simple method to calculate Green's functions for elastic layered media, *Bull. Seism. Soc. Am.*, **71**, 959-971.

Carcione, J.M. & Cavallini, F., 1994. A rheological model for anelastic anisotropic media with applications to seismic wave propagation, *Geophys. J. Int.*, **119**, 338-348.

Carcione, J.M., Kosloff, D. & Kosloff, R., 1988. Wave propagation simulation in a linear viscoelastic medium, *Geophys. J.*, **95**, 597-611.

Day, S.M., 1998. Efficient simulation of constant Q using coarse-grained memory variables, *Bull. Seism. Soc. Am.*, **88**, 1051-1062.

Day, S. M., Bielak, J., Dreger, D., Graves, R., Larsen, S., Olsen, K.B. & Pitarka, A., 2003. *Tests of 3D elastodynamic codes: Final report for Lifelines Project 1A02*, Pacific Earthquake Engineering Research Center, October 10.

Day, S.M. & Bradley, C., 2001. Memory-efficient simulation of anelastic wave propagation, *Bull. Seism. Soc. Am.*, **91**, 520-531.

Day, S.M. & Minster, J.B., 1984. Numerical simulation of wave-fields using a Padé approximant method, *Geophys. J. Roy. Astr. Soc.*, **78**, 105-118.

Dumbser, M., 2005. *Arbitrary High Order Schemes for the Solution of Hyperbolic Conservation Laws in Complex Domains*, Shaker Verlag, Aachen.

Dumbser, M. & Käser, M., 2006. An Arbitrary High Order Discontinuous Galerkin Method for Elastic Waves on Unstructured Meshes II: The Three-Dimensional Isotropic Case, submitted to *Geophys. J. Int.*

Dumbser, M. & Munz, C.D., 2005a. Arbitrary High Order Discontinuous Galerkin Schemes , in *Numerical Methods for Hyperbolic and Kinetic Problems*, eds. Cordier, S., Goudon, T., Gutnic, M. & Sonnendrucker, E., IRMA series in mathematics and theoretical physics, EMS Publishing House, 295–333.

Dumbser, M. & Munz, C.D., 2005b. ADER Discontinuous Galerkin Schemes for Aeroacoustics , in *Comptes Rendus Mécanique*, **333**, 683–687.

Dumbser, M. & Munz, C.D., 2005c. Building Blocks for Arbitrary High Order Discontinuous Galerkin Schemes, *Journal of Scientific Computing*, in press.

Emmerich, H., 1992. PSV-wave propagation in a medium with local heterogeneities: a hybrid formulation and its application, *Geophys. J. Int.*, **109**, 54-64.

Emmerich, H. & Korn, M., 1987. Incorporation of attenuation into time-domain computations of seismic wave fields, *Geophysics*, **52**, 1252-1264.

Graves, R.W., Day, S.M., 2003. Stability and accuracy analysis of coarse-grain viscoelastic simulations, *Bull. Seism. Soc. Am.*, **93**, 283-300.

Käser, M. & Dumbser, M., 2005. An Arbitrary High Order Discontinuous Galerkin Method for Elastic Waves on Unstructured Meshes I: The Two-Dimensional Isotropic Case with External Source Terms. to appear in *Geophys. J. Int.*

Kristek, J. & Moczo, P., 2003. Seismic-Wave Propagation in Viscoelastic Media with Material Discontinuities: A 3D Fourth-Order Staggered-Grid Finite-Difference Modeling, *Bull. Seism. Soc. Am.*, **93**, 2273-2280.

Liu, H. P., Anderson, D. L. & Kanamori, H., 1976. Velocity dispersion due to anelasticity; implications for seismology and mantle composition, *Geophys. J. Roy. Astr. Soc.*, **47**, 41-58.

Luco, J.E. & Apsel, R.J., 1983. On the Green's functions for a layered half-space, Part I, *Bull. Seism. Soc. Am.*, **73**, 909-929.

Marfurt, K.J., 1984. Accuracy of finite-difference and finite-element modeling of the scalar and elastic wave equations, *Geophysics*, **49**, 533-549.

Moczo, P. & Bard, P.Y., 1993. Wave diffraction, amplification and differential motion near strong lateral discontinuities, *Bull. Seism. Soc. Am.*, **83**, 85-106.

Moczo, P., Bystricky, E., Kristek, J., Carcione, J.M. & Bouchon, M., 1997. Hybrid modeling of P-SV Seismic Motion at Inhomogeneous Viscoelastic Topographic Structures, *Bull. Seism. Soc. Am.*, **87**, 1305-1323.

Moczo, P. & Kristek, 2005. On the rheological models used for time-domain methods of seismic wave propagation, *Geophys. Res. Lett.*, **32**, L01306, doi:10.1029/2004GL021598.

Moczo, P., Kristek, J. & Halada, L., 2004. *The Finite Difference Method for Seismologists. An Introduction*, Comenius University, Bratislava.

Reed, W.H. & Hill, T.R., 1973. Triangular mesh methods for the neutron transport equation, Technical Report, LA-UR-73-479, Los Alamos Scientific Laboratory.

Stein, S., 2003. *An Introduction to Seismology, Earthquakes and Earth Structure*, Blackwell Publishing.

Titarev, V.A. & Toro, E.F., 2002. ADER: Arbitrary high order Godunov approach, *J. Sci. Comput.*, **17**, 609-618.

Toro, E.F., 1999. *Riemann Solvers and Numerical Methods for Fluid Dynamics*, Springer, Berlin.
Toro, E.F., Millington, A.C. & Nejad, L.A., 2001. Towards very high order Godunov schemes, in *Godunov methods; Theory and applications*, Kluwer Academic Plenum Publishers, Oxford, 907-940.
Toro, E.F. & Titarev, V.A. 2002. Solution of the generalized Riemann problem for advection-reaction equations, *Proc. Roy. Soc. London*, 271-281.

LIST OF FIGURES